Lab on a Chip

Accepted Manuscript

This article can be cited before page numbers have been issued, to do this please use: A. Sen, S. Peril, M. S and M. Doble, *Lab Chip*, 2015, DOI: 10.1039/C5LC00598A.

ROYAL SOCIETY OF CHEMISTRY

www.rsc.org/loc

View Article Online
DOI: 10.1039/C5LC00598A

Table of contents entry:

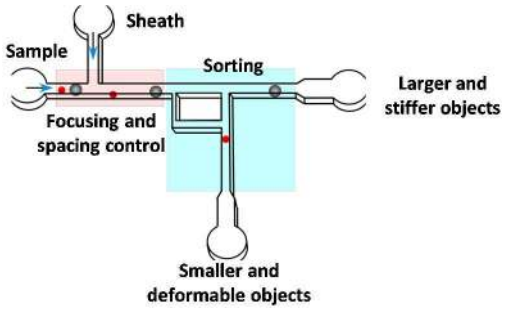

We report a novel hydrodynamic technique for sorting of droplets and cells based on size and deformability

View Article Online
DOI: 10.1039/C5LC00598A

Microfluidic device with focusing and spacing control for resistance based sorting of droplets and cells

P. Sajeesh[1], S. Manasi[2], M. Doble[2], A. K. Sen[1,*]

[1]*Department of Mechanical Engineering, Indian Institute of Technology Madras, Chennai-600036, India*
[2]*Department of Biotechnology, Indian Institute of Technology Madras, Chennai-600036, India*

[*]Author to whom correspondence should be addressed. Email: ashis@iitm.ac.in

Abstract

This paper reports a novel hydrodynamic technique for sorting of droplets and cells based on size and deformability. The device comprises two modules: focusing and spacing control module and sorting module. The focusing and spacing control module enables focusing of objects present in a sample onto one of the side walls of a channel with controlled spacing between them using a sheath fluid. A 3D analytical model is developed to predict the sheath-to-sample flow rate ratio required to facilitate single-file focusing and maintain the required spacing between a pair of adjacent objects. Experiments are performed to demonstrate focusing and spacing control of droplets (size 5-40 μm) and cells (HL60, size 10-25 μm). The model predictions compare well with experimental data in terms of focusing and spacing control within 9 %. In the sorting module, the main channel splits into two branch channels (straight and side branches) with the flow into these two channels separated by a "dividing streamline". A sensing channel and a bypass channel control the shifting of the dividing streamline depending on the object size and deformability. While resistance offered by individual droplets of different size has been studied in our previous work (P. Sajeesh, M. Doble and A. K. Sen, Biomicrofluidics, 2014, 8, 1–23), here we present resistance of individual cells (HL60) as function of size. A theoretical model is developed and used for the design of the sorter. Experiments are performed for size based sorting of droplets (sizes 25 and 40 μm, 10 and 15 μm) and HL60 cells (sizes 11 μm and 19 μm) and deformability based sorting of droplets (size 10±1.0 μm) and polystyrene microbeads (size 10±0.2 μm). The performance of the device for size and deformability based sorting is characterized in terms of sorting efficiency. The proposed device could be potentially used as a diagnostic tool for sorting of larger tumour cells from smaller leukocytes.

1. Introduction

Microfluidics which concerns design, fabrication and experiments of miniaturized fluidic systems, has a number of applications in biomedical, diagnostics and chemical analysis.[1-4] Development of lab on chip (LOC) devices as point-of-care diagnostic tools is one of the pivotal applications of microfluidics.[5] A typical LOC device has various functional modules including sample preparation and transportation module, separation module, detection and analysis module. LOC devices that can sort micron-sized objects such as cells, droplets and particles into distinct populations have found numerous applications in healthcare, research and industry.[6-8] In healthcare, LOC devices are used for disease diagnostics, stem cell research and in mapping of genomes.[9-11] It is possible to detect lethal diseases such as malaria, cancer, and HIV by studying the variation in the physical properties of cells.[12-16] Thus physical properties (size and stiffness) of cells can be considered as important biomarkers that indicate presence of diseases and can be exploited for label-free cell sorting. Epithelial cancer cells are larger in size[15] and more deformable as compared to healthy cells (e.g. MCF 7 and MCF 10A have an order of 1.4-1.8 -times difference in stiffness). Similarly, it has been found that the pancreatic cancer cells have much bigger size as compared to benign cells.[17] Healthy red blood cells (RBCs) are deformable for which they can easily circulate in blood vessels[18] but when infected with malarial parasites, they may block the capillaries due to increase in stiffness (~50 times).[19,20] AFM measurements have shown that sickle cells are smaller in size and of different shape and have higher Young's modulus (~3-times) as compared to healthy cells.[21-23] Thus, size and deformability of cells can be used as biomarkers for the detection of diseases. Besides healthcare, sorting of objects in a sample has importance in the fields of industrial production, food and chemical industry, environmental assessment and chemical or biological research.[24] In digital microfluidics, where droplets are used as microreactors or for encapsulation, sorting of droplets has applications in pharmaceutical, cosmetic, food and material industries.[25] Here, sorting of droplets is essential for precise control of the volume and compositions of various chemicals and to maintain the uniformity of emulsions.

A detailed review of the various active and passive techniques that are used for sorting of microparticles is reported in literature.[8,26] Due to the limitations of the active sorting techniques that make use of biomarkers, antigens or external fields in terms of process, fabrication complexity and cost, label free methods which exploit the physical characteristics of cells

View Article Online
DOI: 10.1039/C5LC00598A

such as size, shape, deformability, and electric or magnetic or optical properties are preferred.[27] Hydrodynamic filtration is a passive sorting technique which was first proposed by Yamada and Seki[28]. In contrast to the conventional filtration methods, hydrodynamic filtration methods offer advantages in terms of reduced chances of clogging. Here, particles are focussed towards one side wall of a channel by continuous withdrawal of liquid through the side wall. In a subsequent work, the device design was modified to include splitting and recombination of flow between the main channel and side channels (on one side) for efficient focusing of particles to the side wall.[29] Later, the device was demonstrated for size based sorting of rat liver cells.[30] Splitting and recombination of flow on both sides of a main channel was used for focusing of particles along the centre of a microchannel.[31] Later, this technique together with a sheath fluid for pinching objects close to a side wall was used for size based sorting of rabbit corneal limbal epithelial cells.[32] One of the limitations of the hydrodynamic filtration method is the complexity of the microchannel network and the design involved. Additionally, the device foot-print is also relatively large. The presence of particles (>0.5-times the channel size) in a segment of microchannel can significantly modify the hydrodynamic resistance and hence the flow distribution.[33-35] Recently, it is demonstrated that the hydrodynamic resistance offered by objects inside a microchannel can be used as a parameter for characterizing the objects based on size and deformability[33,36-38]. Sorting of deformable objects was achieved using the Zweifach–Fung bifurcation law and induced hydrodynamic resistance.[36-38] However, the presence of objects closer to each other (i.e. interacting objects) and at a region away from the channel centre could limit the performance of such devices.

In this paper, we report a novel technique based on the principle of hydrodynamic resistance for sorting of deformable objects based on size and deformability. The device has a focusing and spacing control module and a sorting module. The focusing and spacing control module enables the single-file focusing of objects onto one of the channel walls and controls the spacing between the objects. In literature, hydrodynamic focusing of particles towards the centre of the channel[39,40] or along the side wall[34] has been investigated. In pinched flow fractionation, the particles to be sorted are pinched to one of the side walls using a sheath fluid.[41-43] Although a generalised theoretical model has been derived[44], a theoretical model for focusing and separation control of objects is not reported. The sorting module has a main channel that splits into two branch channels and the flow entering into these two branches is separated by a "dividing streamline". A sensing and a bypass section of the sorting module enables shifting of the dividing streamline depending on the object size and deformability and hence facilitates sorting of objects. Experiments are performed to demonstrate size-based sorting of droplets and HL 60 cells (of same deformability) and finally deformability-based sorting of aqueous droplets and polystyrene microbeads (of same size). First, the sorting device is described and the operating principle is illustrated. Next, three-dimensional analytical models are presented for single-file focusing and spacing control of objects and predicting location of dividing streamline for objects of different size and deformability. Further, the sorter fabrication protocol, experimental setup, materials and methods (for generating emulsions, gelatine droplets and culturing HL60 cells of different size) are detailed. Finally, experimental results for focusing and separation control of objects and size based sorting of droplets and HL60 cells and deformability based sorting of droplets and microbeads are presented and discussed. The performance of the device is characterized based on sorting efficiency.

2. Device description and principle

A schematic of the proposed sorting device and operating principle are illustrated in Fig. 1. The device has two modules (Fig. 1(a)): focusing and spacing control module and sorting module. In the focusing and spacing control module (Fig. 2), the objects present in a sample are focused onto a side wall and the spacing between the objects is controlled using a sheath fluid. The principle of sorting of objects based on size and deformability are presented in Fig. 1(c) and (d), respectively. The sorting technique is based on the principle that at low *Re* (i.e. in the absence of inertial lift forces), an object tend to flow along the streamline passing through its centre of mass.[42]As shown in Fig. 1(b), the main channel bifurcates into two branch channels: straight and side branch channels, with the flow entering into these channels separated by a "dividing streamline". A bypass channel connects the main channel with the side branch channel and the segment of the main channel between the bypass (BPP) and bifurcation points (BRP) is called the "sensing channel". The distance between the dividing streamline and the side wall is called the "critical stream width". In the absence of any object in the sensing channel, the initial critical stream width w_0 depends on the initial flow rate ratio r_i (ratio of flow rates in the straight branch Q_{st} to the side branch Q_{si}). However, this flow rate ratio r changes and hence the critical stream width w is sifted dynamically depending on the size and deformability of the object that arrives at the sensing channel. If the radius of an object r_0 is less than the instantaneous critical stream width w, then the object moves into the side branch, but if the radius of an object r_0 is more than the critical stream width w, then the object continues to move along the straight branch.

The size-based sorting of objects of equal deformability is illustrated in Fig. 1(c). For fixed deformability, the instantaneous flow rate ratio r and hence the instantaneous critical stream width w vary with object size r_0. When a smaller object enters the sensing channel, due to lower resistance change[33], there is a smaller shift in the critical stream width w.

View Article Online
DOI: 10.1039/C5LC00598A

However, when a larger object enters the sensing channel, due to higher resistance change[33], there is a large shift in the critical stream width w. For smaller objects, $w_{sm} > r_0$, thus smaller objects are sorted into the side branch channel. For larger objects, $w_{la} < r_0$, thus larger objects get sorted into the straight branch. A schematic of the variation of w as a function of r_0 is presented (Fig.S1, ESI). As r_0 increases, it offers higher resistance and thus the instantaneous critical stream width w decreases. The object size r_0 for which $w=r_0$ is known as "threshold radius r_t". Thus, objects of size smaller than the threshold object size (i.e. $r_s < r_t$) can be sorted from that of size larger than the threshold size (i.e. $r_l > r_t$). The deformability-based sorting of objects of equal size is illustrated in Fig. 1(d). For fixed size r_0, the instantaneous flow rate ratio r and hence the instantaneous critical stream width w vary with the deformability of objects, which in turn depends on viscosity ratio λ and Young's modulus E_c, respectively, in case of droplets and cells. When a more deformable object enters the sensing channel, due to lower resistance change[33], there is a smaller shift in the critical stream width w. However, when a less deformable or stiffer object enters the sensing channel, due to higher resistance change[33], there is a larger shift in the critical stream width w. For more deformable objects, $w_{de} > r_0$, thus more deformable objects are sorted into the side branch channel. For stiffer objects, $w_{st} < r_0$, thus stiffer objects get sorted into the straight branch. The proposed technique requires that the objects are focused onto the wall and enter into the sensing channel single-file, which is ensured by a sheath fluid (Fig. 2). The extraction of liquid through the bypass channel also helps in the focusing of objects. The bypass flow rate Q_b is very small as compared to the main channel flow rate Q_t thus the critical stream width at bypass channel w_b is much smaller than the object radius, which prevents objects from entering into the bypass channel.

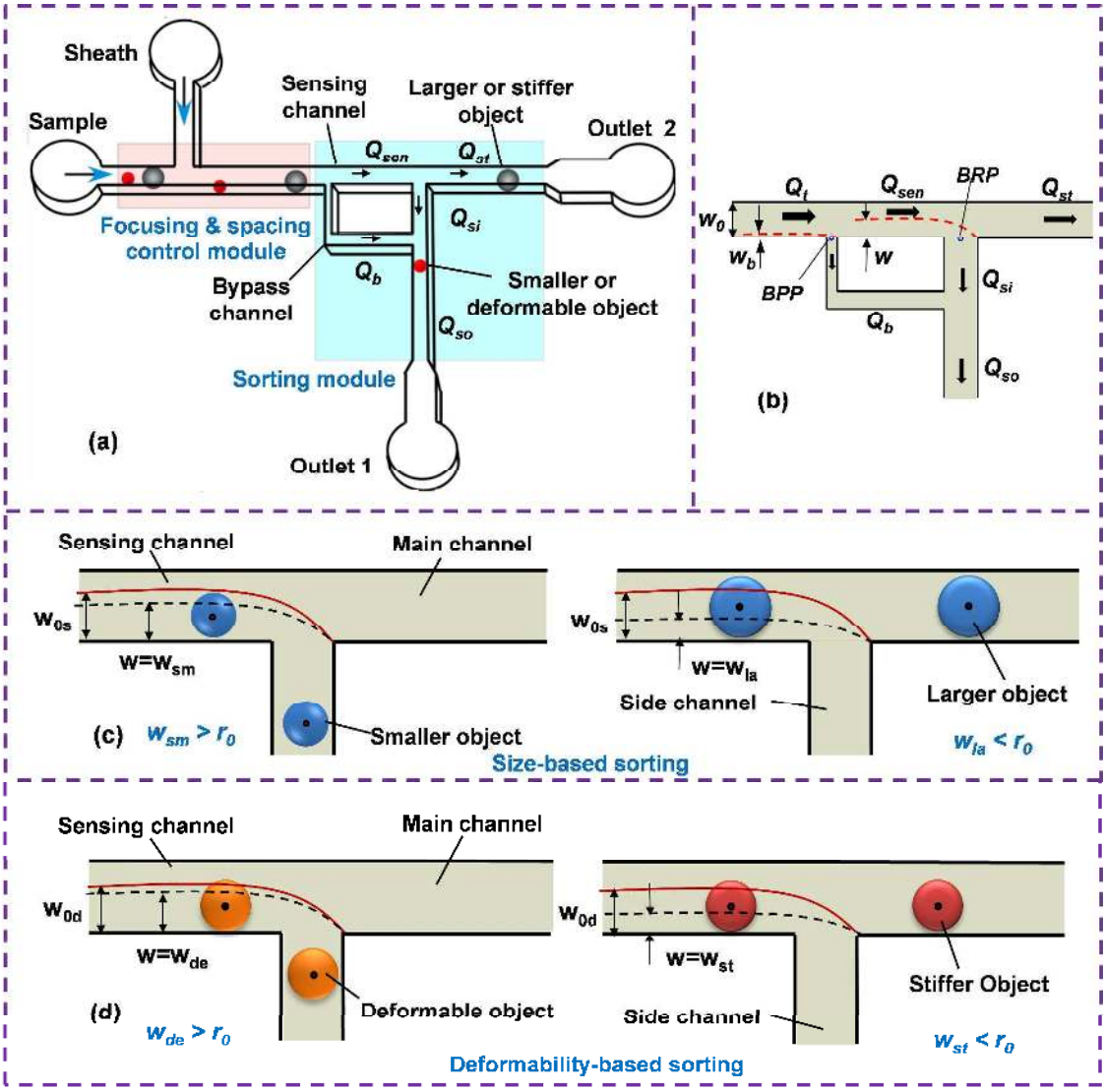

Fig. 1 Schematic of the proposed sorter and operating principle (a) outline of the proposed device (b) relative flow rates in different channel sections (c) sorting based on size (d) sorting based on deformability.

View Article Online
DOI: 10.1039/C5LC00598A

3. Analytical model

3.1 Focusing and spacing control module

The focusing and spacing control module has two distinct regions (Fig. 2). The region *1* is at the upstream in which the objects are randomly distributed across the section. The region *2* is at the downstream in which the sample is subjected to a sheath flow to focus the objects onto the side wall and allow the objects to move single-file. Let size ratio ρ be defined as the ratio of object size d_0 to the characteristic channel size D_c (i.e. hydraulic diameter). Consider a pair of adjacent objects of size ratio ρ_f and ρ_b which are moving at uniform velocities u_{f_1} and u_{b_1}, respectively in region *1*; u_{f_2} and u_{b_2}, respectively in region *2*. Here, the subscript 'f' refers to the leading object and 'b' refers to the trailing object. The subscripts '*1* and *2*' refer to the pair of objects in region *1* and *2*, respectively. The spacing between the objects in region *1* and region *2* are termed as g_1 and g_2, respectively. Consider a situation at which the leading object is about to enter region *2* from region *1* such that the initial spacing between the objects is g_1. As the leading object enters region *2*, it moves at an increased velocity u_{f_2} while the trailing object is still moving at its original velocity u_{b_1} until the trailing object also enters the region *2*. This increase in the velocity of the leading object $(u_{f_2} - u_{f1})$ over a time scale equal to the time taken by the trailing object to reach region *2* is responsible for the increased spacing g_2.

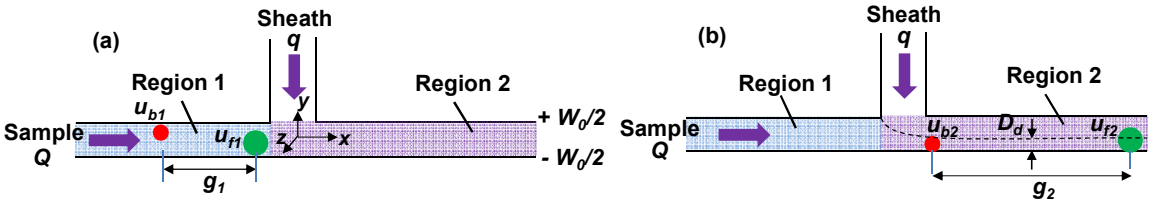

Fig. 2 Schematic of the working principle of focusing and spacing control module (a) before and (b) after the T- junction.

If the required sheath-to-sample flow rate ratio for spacing control is represented as $f_{sc} = \frac{q}{Q}$, the spacing between the objects in region *2* is derived as (detailed derivation in ESI),

$$g_2 = g_1\left(1 + \frac{\phi_{f_2}}{\phi_{b_1}}(1 + f_{sc}) - \frac{\phi_{f_1}}{\phi_{b_1}}\right) \tag{1}$$

where ϕ_{f_1} and ϕ_{f_2} are the mobility[33] of the leading object; ϕ_{b_1} and ϕ_{b_2} are that of the trailing object in region *1* and *2*, respectively.

Next, we derive an expression for the sheath-to-sample flow rate ratio required for focusing of objects of different size. Let D_d be the size of the smallest object to be focused using a sheath-to-sample flow rate ratio $f_p = q/Q$. If we adjust the sheath-to-sample flow rate ratio such that the dividing streamline is located at a distance from the side wall equal to the size of the smallest object then all the objects will be focused onto the side wall. The flow rate ratio $f_p = q/Q$ required for focusing of the objects (of different size) present in a sample is derived as follows (detailed derivation in ESI),

$$D_d(1 + f_p) - W_0 + \sum_{n=odd}^{\infty} \frac{96\,H\,f_p}{\pi^5 n^5}\left[C(B-1) - A\right] - \sum_{n=odd}^{\infty} \frac{96\,H}{\pi^5 n^5}\left[A - C(1+B)\right] = 0 \tag{2}$$

where $A = \sinh\left(\frac{n\pi D_d}{H}\right)$, $B = \cosh\left(\frac{n\pi D_d}{H}\right)$, $C = tanh\left(\frac{n\pi W_0}{2H}\right)$; W_0 and H are width and height of the channel, respectively. The eqn. (2) is solved numerically (using MATLAB) to find out the required flow rate ratio f_p. If the diameter of the object to be focused (or the width of the focused sample stream) is half of the channel width, the above equation predicts that the required flow rate ratio $f_p = 1$, which is expected (i.e. flow rate of both sheath and sample fluids are equal). Finally, in order to achieve the required spacing control as well as object focusing (predicted using eqn. 1 and 2), experiments should be performed at a flow rate ratio $f = \max(f_{sc}, f_p)$.

View Article Online
DOI: 10.1039/C5LC00598A

3.2 Sorting module

A schematic of the microchannel network in the sorting module showing the flow rates in different channel segments and the dividing streamlines at the bypass point (BPP) and branch point (BRP) are depicted in Fig.1(b). An equivalent electrical circuit of this microchannel network is presented (Fig. S2(a), ESI) in which the resistances R_i and currents I_i represent the hydrodynamic resistance and flow rates in different segments of the microchannel network. Using circuit analysis, the equivalent flow rates through different branches of the microchannel network including the flow rates in the side branch channel Q_{si} and straight branch channel Q_{st} are obtained as described (in ESI).

The eqn. (S22, ESI) and (S23, ESI) are combined to establish an equation for the critical stream width w near the branch point in the sensing channel that divides the side branch channel stream from straight branch channel stream as follows,

$$W_0 - w(1+r) + \sum_{n=odd}^{\infty} \frac{96 H r}{\pi^5 n^5}\left[G(F-1) - E\right] + \sum_{n=odd}^{\infty} \frac{96 H}{\pi^5 n^5}\left[E - G(1+F)\right] = 0 \quad (3)$$

where $r = Q_{st}/Q_{si}$ is the ratio of the flow rate in the straight branch channel to the side branch channel and $E = \sinh\left(\frac{n\pi w}{H}\right)$, $F = \cosh\left(\frac{n\pi w}{H}\right)$, $G = tanh\left(\frac{n\pi W_0}{2H}\right)$. The eqn.(3) is solved numerically using MATLAB to determine the critical stream width w (which is also equal to the threshold radius r_t of the object) in a device. The device is designed such that if the radius of an object r_0 is less than r_t, it will be sorted to the side branch channel whereas if $r_0 > r_t$, the object will continue to move along the straight branch channel.

4. Experiments

4.1 Device fabrication

The microchannel devices were fabricated on PDMS using soft lithography. A flexi mask designed in AutoCAD LT 2008 was printed at a resolution of 40,000 dpi (Fineline Imaging Inc, CO, USA). A 4″ silicon wafer (Semiconductor Technology and Application, Milpitas, USA) used as the substrate for photolithography was cleaned (using RCA1, RCA2, and HF dip followed by DI water rinse) and placed in oven for 2.0 min at 120 ^{0}C for removal of moisture. Photoresist SU8 2025 (MicroChem Corp, Newton, USA) was spun coated on to the wafer at 3800 rpm for 30 s with an acceleration of 300 rpm/s. Soft baking was done at 65^{0}C for 1.0 min followed by 95^{0}C for 3.0 min. The photoresist was exposed to UV light (J500-IR/VISIBLE, OAI Mask aligner, CA, USA) through the mask for 15 s. Post exposure bake was done at 65 ^{0}C for 1.0 min followed by 95 ^{0}C for 4.0 min. Finally, the UV-exposed wafer was developed for 6.0 min to obtain the silicon master with SU8 pattern on top of it, which was placed in oven at 100 ^{0}C for 30 min to further improve adhesion between photoresist and wafer. The PDMS soft lithography protocol used for the fabrication of the sorting device is explained elsewhere[33]. The height of the fabricated microchannel was measured using Scanning Electron Microscopy (SEM) and was found to be 19.2 µm and the width of the channel varied depending on the size range of the objects in the sample. Apart from the proposed device, a straight microchannel device of 20×20 µm channel cross-section was also fabricated, which was used for the measurement of the induced hydrodynamic resistance of single cells.

4.2 Materials and methods

4.2.1 Gelatine emulsion

To demonstrate sorting of droplets at higher size range (e.g. 25 µm and 40 µm), glycerol gelatine jelly (Sigma Aldrich, Bangalore) was used as the discrete phase (aqueous glycerol droplets tend to fragment at larger sizes). Glycerol gelatine jelly was first heated to 55-60 ^{0}C to convert it into liquid form. Then, the jelly was mixed with DI water at a concentration of 50% wt/wt and the mixture was heated to 80 ^{0}C. Mineral oil (Thermo fisher scientific India Pvt, Mumbai) was used as the suspending medium for the emulsion. Span 85 (Sigma Aldrich, Bangalore) was added to the mineral oil at a concentration of 5% wt/wt (which is well above Critical Micelle Concentration)[33] as a surfactant to ensure the formation of stable and uniform emulsion. Mineral oil with 5% wt/wt of Span 85 was also heated to a temperature of 80 ^{0}C. Then, 5 µL of the aqueous glycerol gelatine jelly mixture is added to 3.0 mL of oil mixture and mixed (using vortex) at different speeds and for different durations to achieve the required range of gelatine droplet sizes in the emulsion. The emulsion was

View Article Online
DOI: 10.1039/C5LC00598A

suddenly cooled to 4 ^{0}C, which brings the discrete phase gelatine droplets into semi-solid state. Finally, the size and stability of gelatine droplets was ensured (through microscope) before infusing into the device.

4.2.2 Water-in-oil glycerol droplet emulsion

DI water mixed with 80% glycerol was used as discrete phase to form the water-in-oil emulsion. Tween 80 (Sigma Aldrich, Bangalore) was added as a surfactant to this aqueous mixture at a concentration of 0.5 % wt/wt to prevent aggregation of droplets. A 5.0 µL aliquot of the above aqueous mixture was added to 3.0 mL of the oil mixture and mixed (using vortex) at different speeds and for different durations to achieve the required range of droplet sizes in the emulsion. Finally, the size and stability of emulsion was ensured (by observing under a microscope) before infusing into the device.

4.2.3 HL60 cells

HL 60 cells were purchased from NCCS (National Centre for Cell Sciences, Pune, India). The HL 60 cells kept at -80°C were revived with IMDM (Iscove's Modified Dulbecco's Medium) with 20% foetal bovine serum, and were seeded into T 25 flasks with 5.0 mL-20% of the same medium. The cells were grown to confluence in a CO_2 incubator. Then, the cells were sub-cultured in T25 flasks with 10% IMDM, and further incubated for 6.0 h. After that, the cells were transferred into a 15.0 mL falcum tube, and were centrifuged at 1800 rpm for 5.0 min. The supernatant was discarded, and the cells were re-suspended in fresh media before use. Cells of different diameters viz. 10 µm, 15 µm, 20 µm and 25 µm are sorted out using Fluorescence-activated cell sorting (FACS) (FACS ARIA III) with polystyrene beads (Sigma Aldrich, Bangalore) of above size as the standard size for calibration. The number of cells in each sample containing cells of a particular size was counted using a haemocytometer (Marienfeld, Germany)[45]. They were then diluted with IMDM to achieve a final cell concentrations of 1.0 million/mL. These cell samples (each containing cells of a fixed uniform size) are used to determine the induced hydrodynamic resistance of individual cells as a function of cell size.

4.3 Experimental set up

Initially, experiments were performed to measure the induced hydrodynamic resistance of single cells using the experimental setup and procedure reported earlier[33]. The hydrodynamic resistance of HL60 cells of different size (10-25 µm) was measured and used for design of the sorting device. Gelatine and aqueous glycerol droplets (in mineral oil) and HL60 cells (in IMDM) were used as the sample to demonstrate sorting. In the case of gelatine and aqueous glycerol droplets, mineral oil was used as the sheath fluid whereas for HL60 cells, IMDM was used as the sheath fluid. The sample and the sheath fluids were infused into the device using a syringe pump (TSE systems, Germany). An inverted microscope (Carl Zeiss Axiovert A1) coupled with a high-speed camera (Photron FASTCAM SA3) interfaced with PC via Photron FASTCAM viewer software was used for observation and capture of images of objects inside the device. The experiments were performed at the required flow rate ratio f (ref. section 3.1) for focusing and spacing control of objects depending on the concentration and size of the objects to be sorted. In the experiments, the spacing between the objects in region *1* and *2* and focusing of the objects near the wall in region *2* of the focusing and spacing control module was observed at different flow rate ratios. The shifting of the diving streamline near the sorting junction is demonstrated using fluorescent dye. The sorting of objects of different size into the side and straight branches are captured using high speed camera (1000fps).

5. Results and Discussion

5.1 Size control of objects

The size of droplets was controlled by adjusting the vortex speed and duration of mixing of gelatine or aqueous glycerol with mineral oil (with surfactant for stability). At a vortex speed of 2500 rpm for 2 min, the aqueous glycerol droplets were observed to be in the size range 2-35 µm (Fig. S3 (a), ESI). When the same mixture is vortexed at a speed of 2500 rpm for 5.0 min, aqueous glycerol droplets were obtained with a size range of 9-11 µm. Similarly at a speed of 2000 rpm for 1.0 min, the gelatine droplets had size in the range 10-60 µm. The number density of droplets in the emulsion was controlled by adjusting the volume ratio of the gelatine or aqueous glycerol to mineral oil in the mixture. The number density of the emulsion used in our experiments was such that the minimum distance between any two adjacent droplets is more than the channel size so that droplet-droplet interaction can be ignored.[34] The size contrast of HL60 cells (ESI) was studied by varying the cell culture time in the range 2-24 h. The cell line which was cultured for ~6.0 h showed wide variation of cell size (with a minimum cell size of 8.9 µm and maximum cell size of 25 µm, and average cell size 14.58 µm) as depicted (Fig. S3 (b) and (c), ESI). But, when the cells were cultured for ~24 h, it showed a more uniform size (in the range 11.97±1.96 µm), (Fig. S3 (d), ESI).The cells cultured for 6 h were sorted according to size using FACS to obtain cells of size 10µm, 15µm, 20µm and 25µm. The sorted cell sample of each individual size are further cultured for >24 h to

View Article Online
DOI: 10.1039/C5LC00598A

increase the cell concentration. The concentrated cell samples had uniform size i.e. cultured 10 µm cell sample have a size of 10±1 µm and similarly, the 15 µm, 20 µm and 25 µm cells showed a variation of ±1, ±1 and ±0.8, respectively.

5.2 Focusing of objects

To ensure focusing of objects of different size onto the side wall, sheath-to-sample flow rate ratio f is adjusted so that the sample stream width is equal to the diameter of the smallest object. The focusing of droplets (aqueous glycerol) in the size range 6-14 µm using mineral oil is presented (Fig. S5(a), ESI). Using a sheath-to-sample flow rate ratio of 3.45, the width of the focused sample stream is adjusted to 6.0 µm such that all droplets get focused onto the side wall. Irrespective of the initial position of the objects across the channel cross-section, the objects get focused onto the side wall as shown (Fig. S5(b), ESI). Optical images of focusing of a cluster of droplets due to the sheath fluid and subsequently their position at a different location downstream is presented (Fig. S5(c), ESI). The variation of the required flow rate as a function of the minimum object size to be focused obtained from the analytical model (eqn. (2)) and measured from experiments are presented in Fig. 3. As observed, the required flow rate ratio increases with decrease in the minimum size of the droplets to be focused. A good match (within 8%) between the analytical and experimental results is observed.

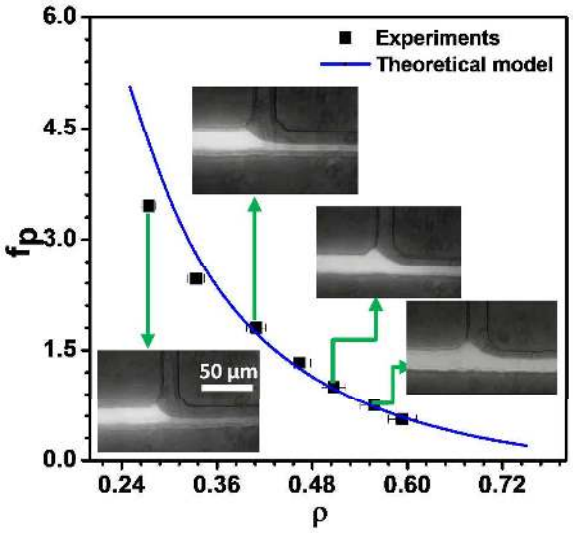

Fig. 3 Comparison of experimental data with predictions of the analytical model for the flow rate ratio $f_p = q/Q$ required for focusing of droplets of various size ratios $\rho = d_0/D_c$.

5.3 Spacing control of objects

The sheath fluid is used to control spacing between pair of adjacent objects. The initial spacing between objects in region *1* i.e. g_1 is inversely proportional to the sample concentration (Fig. S3(b) and (c), ESI). The sheath-to-sample flow rate ratio f required to achieve spacing higher than the length of the sensing channel L_{sen} is directly proportional to the initial sample concentration. The variation of spacing ratio $g^* = g_2/g_1$ with flow rate ratio f for different relative size ratio ρ_r (i.e. the ratio of diameter of the leading object to that of the trailing object in a pair of objects) measured from experiments and predicted using the model is depicted in Fig. 4. It is observed that spacing ratio g^* increases linearly with increase in flow rate ratio f and the match between the analytical model and experimental data is within 9%. It is interesting to note that flow rate ratio f_{sc} required to maintain a particular spacing ratio g^* between the pair of objects having relative size ratio ρ_r =0.5 is 11-12% lower than that for a pair of objects having relative size ratio ρ_r =1. Similarly, for ρ_r =1.5, about 6 % higher flow rate ratio is required for maintaining a particular spacing ratio as compared to ρ_r =1. A detailed explanation of these observations obtained from experiments and VOF simulations is reported (spacing control of objects, ESI).

View Article Online
DOI: 10.1039/C5LC00598A

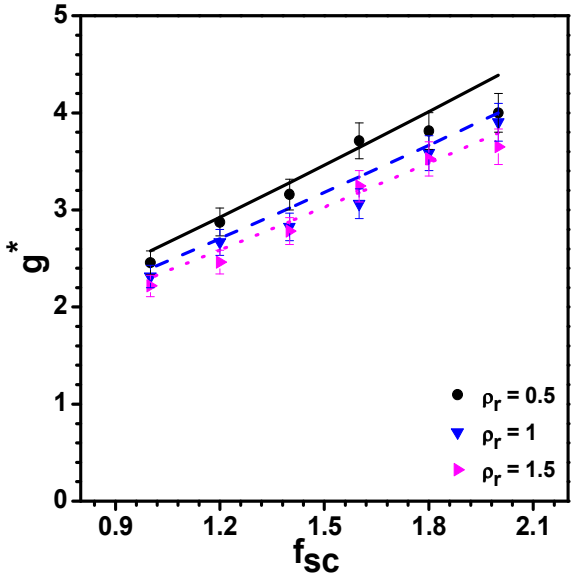

Fig. 4 Spacing ratio of a pair of adjacent objects as a function of the flow rate ratio for different relative size ratios ρ_r : comparison between experimental data (shown by symbols with error bars) and predictions of the analytical model (shown by solid line, dashed line and dotted line for ρ_r =0.5, 1.0 and 1.5, respectively).

5.4 Induced hydrodynamic resistance and mobility of single cells

Earlier, we had reported induced hydrodynamic resistance of droplets as a function of their size and viscosity ratio[33]. We had also reported bulk hydrodynamic resistance of polystyrene microbeads and various biological cells. Here, we performed experiments to measure induced hydrodynamic resistance of individual HL60 cells of different size in the range 10-25 µm by using a similar procedure which was reported earlier. The variation of resistance of individual cells as a function of cell size is depicted in Fig. 5. As observed, the induced hydrodynamic resistance increases with increase in the cell size. Since, the size of the cells are comparable to that of the channel size (~20µm), for a larger cells, there is higher viscous dissipation in the thin layer of liquid between the cell membrane and the channel wall, which leads to higher resistance. Also, it is interesting to observe that the resistance offered by a cell is higher than that of a droplet of same size[33] which may be due to the higher stiffness of the cells as compared to droplets. The induced hydrodynamic resistance can be correlated with cell size as $\Delta R_d / R \sim f(E_o)\rho_c^n$, where ρ_c is the size ratio of cells (i.e. ratio of cell size to the characteristic channel size d_c / D_c) and E_o is the Young's modulus of HL60 cells, which is reported to be in the range 0.2-1.4 kPa.[47] For sorting of cells of different size but same stiffness (assuming that Young's modulus is independent of cell size), the induced hydrodynamic resistance is correlated with cell size as follows,

$$\frac{\Delta R_d}{R} = K\,\rho_c^n \tag{4}$$

Where $K = 0.0739$ and $n = 3.03$. This correlation was found by curve fitting of experimental data in MATLAB with R^2 value of 0.85 and 95% confidence bound.

View Article Online
DOI: 10.1039/C5LC00598A

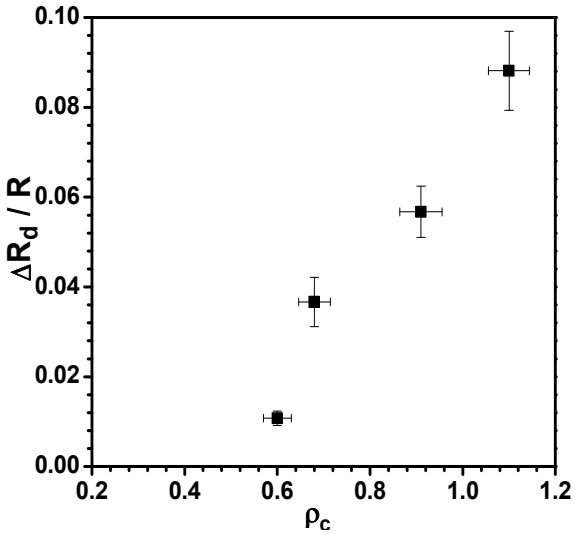

Fig. 5 Variation of induced hydrodynamic resistance of individual cells $\frac{\Delta R_d}{R}$ with the size ratio ρ_c of the cells

5.5 Sorting of droplets and cells

The design of the sorter is based on the analytical model reported in section 3.2 and described in (sorting of droplets and cells, ESI). The sorting devices were used for size based sorting of gelatine droplets of size ≤25 μm from those ≥40 μm, aqueous glycerol droplets of size ≤10 μm from those ≥15 μm, and HL60 cells of size ≤12 μm from cells of size ≥17 μm. The variation of the critical width with object size for gelatine droplets, aqueous glycerol droplets and HL60 cells are depicted (Fig. S7, ESI). Finally, we demonstrate sorting of droplets from polystyrene microbeads of equal size which have distinct stiffness (and hence induced hydrodynamic resistance), as reported in our earlier work.[33]

First, experiments were performed with the sorting device to sort gelatine droplets of size ≤25 μm from those ≥40 μm, as shown in Fig. 6 (a) and (b). In the absence of any droplets in the sensing channel, the unperturbed critical width was calculated to be 22μm. When a droplet of size (diameter) 25 μm enters the sensing channel, the critical width is dynamically reduced to 21 μm (dynamic control of the critical stream width shown in Fig. S8, ESI). Since the radius of the droplet is less than the instantaneous critical width, the 25 μm droplets are sorted into the side branch channel. However, when a droplet of size (diameter) 40μm arrives at the sensing channel, the critical width is dynamically reduced to 9 μm. Now, since the radius of the droplet is higher than the instantaneous critical width, the 40 μm droplets are sorted into the straight channel. The performance of the device in terms of sorting efficiency for sorting of droplets of different size is depicted in Fig. 6(c). The sorting efficiency was found to be between 70 to 94% depending on the droplet size contrast. The sorting of aqueous glycerol droplets of 10 μm size from that of 15 μm size using VOF simulations and experiment are also depicted (Fig. S9 and S10, ESI).

Next, experiments were performed for sorting of HL 60 cells. In this case, the critical stream width is 6.0 μm thus the device is capable of sorting HL60 cells of size smaller and larger than 12 μm. For cells of size <12 μm, the cell radius is lower than the dynamic critical stream width and thus sorted into the side branch channel. However, for the cells of size >12 μm, the cell radius is higher than the dynamic critical stream width and thus sorted into the straight branch channel. The results showing sorting of HL60 cells of 11 μm size from those of 19 μm size are depicted in Fig. 7(a) and (b). The performance of the device is characterised in terms of cell sorting efficiency. The sorting efficiency is defined as the ratio of the number of cells of a particular size collected at an outlet to the total number of cells of the same size infused into the device within a stipulated time. The cell sorting efficiency was found out by using a mixture of cells of size in the range 10-25 μm and the results are depicted in Fig. 7(c). The sorting efficiency of the device (about a threshold cell size of 12 μm) is found to be between 80 to 97% depending on the relative sizes of the cells being sorted. For example, the sorting efficiency of the device for sorting of cells of 11 μm size from a mixture of cells >12 μm is around 80% whereas the sorting efficiency of the device for sorting of cells of 20 μm size from cells of size <12 μm is found to be around 97%.

Finally, we perform experiments to demonstrate sorting of objects based on their deformability contrast. Here, we demonstrate sorting of droplets from polystyrene microbeads of same size. Experimental images showing the trajectory droplets of 15 μm size from polystyrene microbeads (of 15 μm size) are presented in Fig. 8(a) and (b). As discussed earlier

View Article Online
DOI: 10.1039/C5LC00598A

and observed in our earlier work[33], the induced hydrodynamic resistance of droplets is much lower as compared to that of microbeads. Thus, for droplets present in the sensing channel, the critical stream width is higher than the radius of the droplets (i.e. 7.5 μm) due to which the droplets are sorted into the side branch channel. On the other hand, in case of microbeads, the critical stream width is smaller as compared to the radius of the microbeads thus the microbeads are sorted into the straight branch channel. The performance of the device in terms of sorting efficiency for deformability based sorting of polystyrene microbeads of size 10±0.2 μm from droplets of size 10±1.0 μm (and viscosity ratio λ in the range 0.032-1.467) is depicted in Fig. 8(c). The slight difference in the size of the beads and droplets is found to have negligible effect on the sorting behaviour (since this small size difference provides negligible difference in the resistance change[33]), so the sorting efficiency is solely due to the difference in their deformability. The sorting efficiency was found to be between 70 to 90% depending on the deformability contrast between the beads and the droplets of different viscosity ratio λ. Sorting of different types of cells (of same size) based on the difference in their stiffness is beyond the scope of the present work and we plan to investigate this in future.

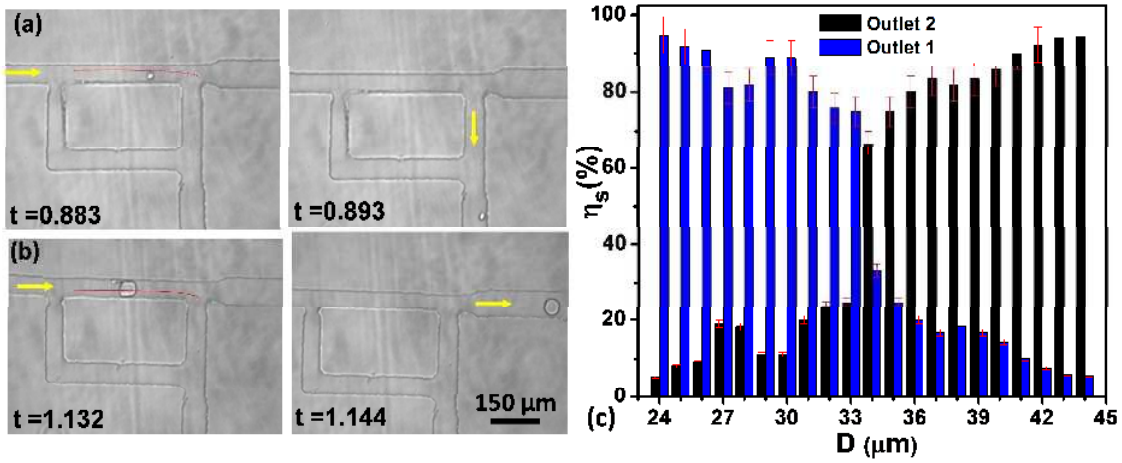

Fig.6 Experimental images showing (a) trajectory of droplets <20 μm diameter sorted to the side branch channel (b) trajectory of droplets >40 μm diameter continue to move in the main channel, position of dividing streamlines also shown(c) Performance of the device in terms of sorting efficiency for different diameter of droplets.

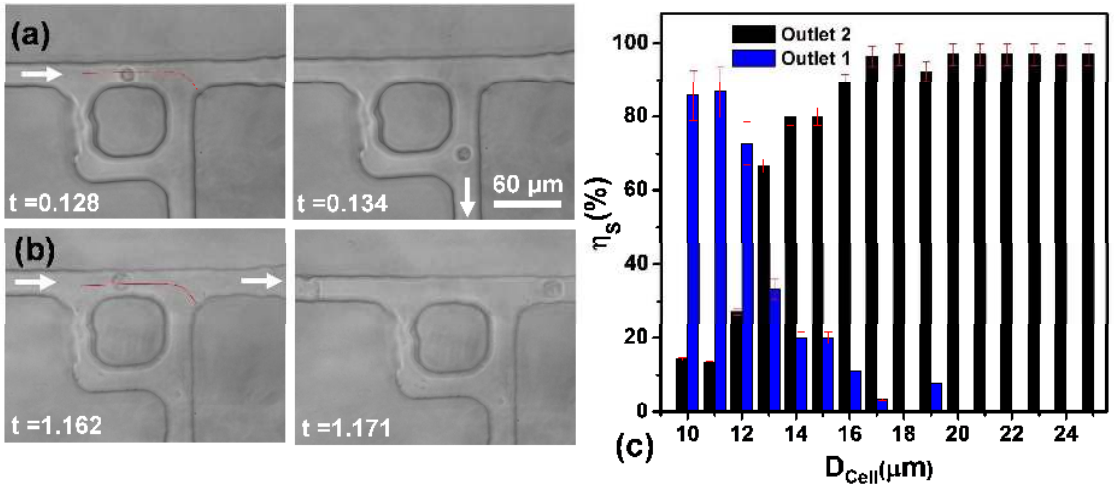

Fig. 7 Experimental images showing the trajectory of HL 60 cells (a) of diameter 11μm sorted to the side branch channel (b) of diameter 19 μm sorted to the straight branch channel, position of dividing streamlines shown (c) Performance of the device in terms of sorting efficiency for different diameter of cells.

View Article Online
DOI: 10.1039/C5LC00598A

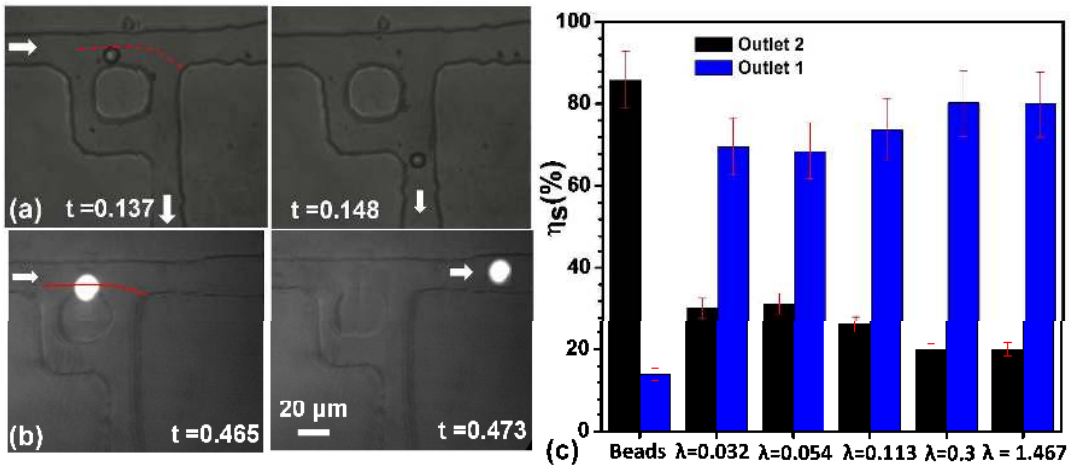

Fig. 8 Experimental images showing trajectory of (a) aqueous glycerol droplets of diameter 15µm (b) fluorescent polystyrene microbeads of diameter 15µm objects, position of dividing streamlines had shown (c) Performance of the device in terms of sorting efficiency for different stiffness of objects from the polystyrene beads of same diameter (10 µm).

7. Conclusion

We presented a novel hydrodynamic technique for sorting of droplets and cells based on size and deformability. The proposed device has a focusing and spacing control module and a sorting module. The focusing and spacing control module in the upstream of the device enables focusing of objects onto the channel side wall and control of spacing between a pair of adjacent objects, which are essential for sorting of objects in the sorting module downstream. Experiments were performed to demonstrate focusing of objects of different size present in a sample using a sheath fluid. It was observed that the required sheath-to-sample flow rate ratio decreases with increase in the object size. A 3D analytical model predicts the flow rate ratio required for the focusing of objects of different size. The results of the experiments and predictions of the analytical model were compared which was found to match well (within 8%). Experiments were performed to investigate the control of spacing between a pair of adjacent objects (of different relative size ratio i.e. ratio of the leading to trailing object size) present in a sample using a sheath fluid. The results showed that the spacing between a pair of adjacent objects increases with increase in the sheath-to-sample flow rate ratio. Also, it observed that for a fixed flow rate ratio, the spacing between the objects is higher for a lower relative size ratio. An analytical model was derived to predict the spacing control between a pair of objects of different relative size ratio. The prediction of the analytical model compared well (within 9%) with the experimental data. Induced hydrodynamic resistance offered by individual HL 60 cell inside a microchannel of comparable size was studied which was found to increase with increase in the size ratio of the cells. Similarly, the induced hydrodynamic resistance of a cell is observed to be higher as compared a droplet of same size. A 3D analytical model was derived which was used for design of the sorting module. The model was used to determine the critical stream width for gelatine droplets, aqueous glycerol droplet and HL60 cells of different size. Sorting of gelatine droplets of size ≤25 µm from those of size ≥40 µm and aqueous glycerol droplets of size ≤10 µm from those of size ≥15 µm was demonstrated. The device was then demonstrated for sorting of HL60 cells of size ≤12 µm from those of size ≥17 µm. To characterize performance of the device, sorting efficiency was determined for a mixture of cells in the range 10-25 µm, which was found to be in the range 80-97% depending on the cell size. Finally, the device was used for sorting of objects based on stiffness by sorting droplets and polystyrene microbeads of size. The sorting efficiency for the deformability based sorting was found to be between 70 to 90% depending on the deformability contrast of objects. In our future work, we plan to use the device for sorting of different cells of equal size but different stiffness. The proposed device could be potentially used for sorting of diseased cells from healthy cells.

Acknowledgements

The authors would like to thank the Department of Biotechnology (DBT), India for providing the financial support for the project. We also acknowledge MEMS Lab of EE, IIT Madras for supporting the photolithography work. The authors also thank the Department of Metallurgy, IIT Madras for the SEM characterization of the channels.

View Article Online
DOI: 10.1039/C5LC00598A

References

1. P. K. Sahu, A. Golia and A. K. Sen, Microsyst. Technol., 2012, **19**, 493–501.
2. A. K. Sen, J. Darabi and D. R. Knapp, Sensors Actuators B Chem, 2010, **137**, 789–796.
3. A. K. Sen, T. Harvey and J. Clausen, Biomed. Microdevices, 2011, 13, 705–715.
4. J. Voldman, M. L. Gray and M. A. Schmidt, Annu. Rev. Biomed. Eng., 1999, **1**, 401–425.
5. G. M. Whitesides and A. D. Stroock, Phys. Today, 2001, **54**, 42–48.
6. P. Bhardwaj, P. Bagdi and A. K. Sen, Lab Chip, 2011, **11**, 4012.
7. M. Kersaudy-Kerhoas, R. Dhariwal and M. P. Y. Desmulliez, Nanobiotechnology, IET, 2008, **2**, 1–13.
8. P. Sajeesh and A. K. Sen, Microfluid. Nanofluidics, 2013, **17**, 1–52.
9. E. Y. Chan, N. M. Goncalves, R. A. Haeusler, A. J. Hatch, J. W. Larson, A. M. Maletta, G. R. Yantz, E. D. Carstea, M. Fuchs, G. G. Wong, S. R. Gullans and R. Gilmanshin, Genome Res., 2004, 1137–1146.
10. Y. C. Toh, C. Zhang, J. Zhang, Y. M. Khong, S. Chang, V. D. Samper, D. van Noort, D. W. Hutmacher and H. Yu, Lab Chip, 2007, **7**, 302–9.
11. D. Wlodkowic and Z. Darzynkiewicz, World J. Clin. Oncol., 2010, **1**, 18–23.
12. M. Alshareef, M. Nicholas, E. J. Perez, F. Azer, F. Yang, X. Yang and G. Wang, Biomicrofluidics, 2013, **7**, 11803.
13. R. A. Harouaka, M. Nisic and S. Y. Zheng, J Lab Autom., 2013, **18**, 1–24.
14. S. Suresh, ActaBiomater., 2007, **3**, 413–438.
15. S. Suresh, J. Spatz, J. P. Mills, a Micoulet, M. Dao, C. T. Lim, M. Beil and T. Seufferlein, ActaBiomater., 2005, **1**, 15–30.
16. A. Vaziri and A. Gopinath, Nat Mater, 2008, **7**, 15–23.
17. L. J. Edens, K. H. White, P. Jevtic, X. Li and D. L. Levy, Trends Cell Biol., 2013, **23**, 151–159.
18. M. Mak and D. Erickson, Integr. Biol. (Camb)., 2013, **5**, 1374–84.
19. H. A. Cranston, C. W. Boylan, G. L. Carroll, S. P. Sutera, Williamson, I. Y. Gluzman and D. J. Krogstad, Sci. , 1984, **223** , 400–403.
20. J. P. Shelby, J. White, K. Ganesan, P. K. Rathod and D. T. Chiu, 2003, **100**, 14618–14622.
21. M. Diez-Silva, M. Dao, J. Han, C. T. Lim and S. Suresh, MRS Bull., 2010, **35**, 382–388.
22. J. L. Maciaszek, B. Andemariam and G. Lykotrafitis, J. Strain Anal. Eng. Des., 2011, **46**, 368–379.
23. J. L. Maciaszek and G. Lykotrafitis, J. Biomech., 2011, **44**, 657–661.
24. D. R. Reyes, D. Iossifidis, P. A. Auroux and A. Manz, Anal. Chem., 2002, **74**, 2623–2636.
25. D. R. Link, E. Grasland-Mongrain, A. Duri, F. Sarrazin, Z. Cheng, G. Cristobal, M. Marquez and D. A. Weitz, Angew. Chem. Int. Ed. Engl., 2006, **45**, 2556–60.
26. N. Pamme, Lab Chip, 2007, **7**, 1644.
27. A. Karimi, S. Yazdi and A. M. Ardekani, Biomicrofluidics, 2013, **7**, 21501.
28. M. Yamada and M. Seki, Lab Chip, 2005, **5**, 1233–1239.
29. M.Yamada and M. Seki, Anal. Chem., 2006, **78**, 1357–1362.
30. M. Yamada, K. Kano and Y. Tsuda, Biomed Microdevices, 2007, **9**, 637–645.
31. R. Aoki, M. Yamada, M. Yasuda and M. Seki, Microfluid. Nanofluidics, 2008, **6**, 571–576.
32. A. Hasegawa, M. Yamada, M. Seki, M. Yamato and T. Okano, International Symposium on Micro-Nano Mechatronics and Human Science (MHS), IEEE, 2013, 1–5.
33. P. Sajeesh, M. Doble and A. K. Sen, Biomicrofluidics, 2014, 8, 1–23.
34. H. Brenner, J. Fluid Mech., 1970, **43**, 641–660.
35. D. A. Sessoms, M. Belloul, W. Engl, M. Roche, L. Courbin and P. Panizza, Phys. Rev. E, 2009, **80**, 1–10.
36. M. A. C. Ayala, M.Raafat and R. Karnik, Small, 2013, **9**, 375-381.
37. M. S. Raafat, M. C. Ayala and R. Karnik, in 14th International Conference on Miniaturized Systems for Chemistry and Life Science, 2010, 1826–1828.
38. M. S. Raafat, M.S. Thesis, Massachusetts Institute of Technology, 2010.
39. J. B. Knight, A. Vishwanath, J. P. Brody and R. H. Austin, Phys. Rev. Lett., 1998, **80**, 3863–3866.
40. T. Stiles, R. Fallon, T. Vestad, J. Oakey, D. W. M. Marr, J. Squier and R. Jimenez, Microfluid. Nanofluidics, 2005, **1**, 280–283.
41. H. Maenaka, M. Yamada, M. Yasuda and M. Seki, Langmuir, 2008, **24**, 4405–4410.
42. M. Yamada, M. Nakashima and M. Seki, Anal. Chem., 2004, **76**, 5465–5471.
43. J. Takagi, M. Yamada and M. Seki, Lab Chip, 2005, **5**, 778–784.
44. K. B. Andersen, S. Levinsen, W. E. Svendsen and F. Okkels, Lab Chip, 2009, **9**, 1638–1639.
45. G. Venkatachalam, V. Nandakumar, G. Suresh and M. Doble, RSC Adv., 2014, **4**, 11393.
46. J. Happel and H. Brenner, Low Reynolds Number Hydrodynamics: With Special Applications to Particulate Media, Springer Netherlands, 1983.
47. T. G. Kuznetsova, M. N. Starodubtseva, N. I. Yegorenkov, S. A. Chizhik and R. I. Zhdanov, Micron, 2007, **38**, 824–33.